Nationaal Lucht- en Ruimtevaartlaboratorium

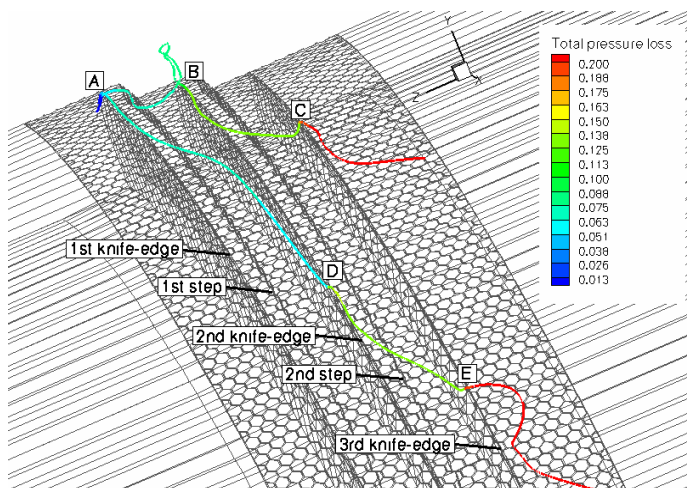National Aerospace Laboratory NLR

Executive summary

Performance evaluation of gas turbine labyrinth seals using computational fluid dynamicss

Problem area

Increasing performance requirements on gas turbines have led to ever increasing gas temperatures and pressure ratios. Together with the resulting increase in cooling flows, this requires internal gas leakages to be minimized and controlled even further.

The application of new seal designs and improved understanding of leakage flow characteristics are of particular importance in order to meet future performance goals.

Labyrinth seals, despite their unavoidable leakage, remain the most common seal types in modern gas turbines. The combination of high rotational speeds, high gas temperatures and high pressure differences often precludes the use of other seal types, and the labyrinth seal remains the only choice to meet reliability and durability standards of modern engines.

Understanding the flow in labyrinth seals at engine compliant conditions is fundamentally important in developing improved seal concepts to enhance and predict component performance in gas turbines engines.

Obtaining such an understanding is part of a mission to bring new gas turbine labyrinth seal concepts to a higher level of technology readiness for advanced propulsion and power systems.

Simulation methods based on Computational Fluid Dynamics

This report is based on a presentation held at the ASME Turbo Expo 2007: Power for Land, Sea and Air, Montreal (Canada), 14-17 May, 2007.

Performance evaluation of gas turbine labyrinth seals using computational fluid dynamicss

(CFD) have gained significant interest in recent years. Apart from its potential to reduce risks involved during the development process of a new seal, CFD allows one to gain a thorough insight into the flow processes inside the seal. The continuing development of CFD algorithms, facilitated by the ever increasing performance and cost-effectiveness of computers, opens ample possibilities to incorporate more complete physics into the CFD modeling.

Description of work

The focus of the paper lies in the application of CFD to assess labyrinth seals. The Reynolds-Averaged Navier-Stokes equations are employed as the flow governing equations, with turbulence incorporated through the TNT variant of the k-ω turbulence model.

The first objective of this paper is to perform a comparison between numerical and experimental results, involving CFD computations for a three-dimensional labyrinth seal with a honeycomb land that closely represents a tested seal model.

Subsequently, the computational results facilitate a three-dimensional investigation to get a good insight into the flow phenomena in the labyrinth seal. The second objective is therefore to present a new approach for exploiting the CFD methodology to investigate the flow characteristics and sealing mechanisms in terms of losses generated in the labyrinth seals.

The third objective is to demonstrate the suitability of the approach for assessing different seal concepts.

Results and conclusions

The comparison between the results of the CFD computation and the experimental measurement shows a close agreement. This is a strong indication that the important flow physics responsible for the sealing mechanism have been captured by the CFD method.

An analysis of the flow topology and the losses experienced along the streamlines reveals that the sealing mechanism of the flow through labyrinth seals is due to losses associated with turbulent mixing and shear which dominantly occur in the vicinity of the knife edge and to a lesser extent around the step wall. The effects of the honeycomb cells can be identified as decreased production of losses.

Applicability

The CFD method is considered as an analysis tool complementary to rig-testing and enables investigating the effect of new seal design features. Additionally CFD is seen as a tool to support the correct representation of test-data in semi-empirical engineering models for seal design. An industrial perspective is foreseen towards an extensive exploitation of the CFD modeling capabilities for real-life design of seals.

NLR-TP-2007-624

Performance evaluation of gas turbine labyrinth seals using computational fluid dynamicss

B.I. Soemarwoto, J.C. Kok, K.M.J. de Cock, A.B. Kloosterman, G.A. Kool and J.F.A. Versluis[1]
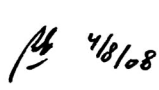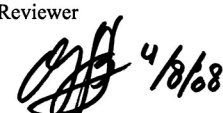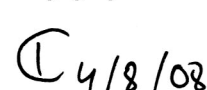
[1] Sulzer Metco Turbine Components

The contents of this report may be cited on condition that full credit is given to NLR and the authors.

This publication has been refereed by the Advisory Committee AEROSPACE VEHICLES.

Customer	National Aerospace Laboratory NLR
Contract number	----
Owner	National Aerospace Laboratory NLR
Division	Aerospace Vehicles
Distribution	Unlimited
Classification of title	Unclassified
	July 2008

Approved by:

Author	Reviewer	Managing department
4/8/08	*4/8/08*	*4/8/08*

Summary

The paper presents an investigation on the characteristics of flow through labyrinth seals. The focus of the paper lies in the application of the Computational Fluid Dynamics (CFD) methodology. The Reynolds-Averaged Navier-Stokes equations are employed as the flow governing equations. Turbulence is incorporated through a variant of the two-equation k-ω turbulence model.

Three test cases are considered. The first test case concerns a labyrinth seal configuration with a honeycomb land. The computational results are compared to those obtained from seal test rig measurements. The second test case addresses the same labyrinth seal where the honeycomb land is replaced by a solid smooth land. The third test case addresses the flow through a labyrinth seal with canted knives.

The CFD method is considered as an analysis tool complementary to rig-testing and enables investigating the effect of new seal design features. Additionally CFD is seen as a tool to support the correct representation of test-data in semi-empirical engineering models for seal design. An industrial perspective is presented towards the exploitation of these modeling capabilities for real-life design of seals.

Contents

Abbreviations

A	inlet area (m^2)
A_{gap}	circumferential gap area of the first knife (m^2)
p	pressure ($N|m^2$)
p_i	inlet pressure ($N|m^2$)
p_o	outlet pressure ($N|m^2$)
p_t	total pressure ($N|m^2$)
$p_{t,ref}$	reference total pressure specified at the inlet ($N|m^2$)
$p_{t,loss}$	total pressure loss ($N|m^2$)
T	temperature (K)
T_i	inlet temperature (K)
u	axial inlet velocity ($m|s$)
W	mass flow ($kg|s$)
M	Mach number
ρ	density ($kg|m^3$)
ϕ	mass flow function ($kg\,K^{1/2}|N|s$)
Π	pressure ratio
γ	ratio of specific heats, $\gamma = 1.4$

This page is intentionally left blank.

1 Introduction

Increasing performance requirements on gas turbines have led to ever increasing gas temperatures and pressure ratios. Together with the resulting increase in cooling flows, this requires internal gas leakages to be minimized and controlled even further. The application of new seal designs and improved understanding of leakage flow characteristics are of particular importance in order to meet future performance goals. Labyrinth seals, despite their unavoidable leakage, remain the most common seal types in modern gas turbines. The combination of high rotational speeds, high gas temperatures and high pressure differences often precludes the use of other seal types, and the labyrinth seal remains the only choice to meet reliability and durability standards of modern engines.

Understanding the flow in labyrinth seals at engine compliant conditions is fundamentally important in developing improved seal concepts to enhance and predict component performance in gas turbines engines. Obtaining such an understanding is part of a mission to bring new gas turbine labyrinth seal concepts to a higher level of technology readiness for advanced propulsion and power systems.

To accomplish such a mission, three technological blocks can be identified at NLR consisting of (i) an experimental method facilitated by an advanced seal test rig, (ii) a numerical method based on Computational Fluid Dynamics (CFD), and (iii) a semi-empirical engineering model. The seal test rig (Ref. 1) has the advanced capability to simulate flows through a highly representative seal model at extreme engine conditions such as high temperatures, high rotational speeds and high pressures to which prospective advanced seals are exposed. Additionally, the test data from such a seal test rig support the enhancement and validation of engineering model and CFD methodology.

Simulation methods based on CFD have gained significant interest in recent years. This trend is reflected in the literature. However, previous works were limited to simplified cases, where important geometrical features (such as a complete description of the honeycomb cells) and/or flow conditions (such as the rotation) were not included. For example, Ref. 2 presented CFD computations on a simplified rotating knife on a smooth land, i.e. without honeycomb cells. Ref. 3 presented an approach to include the effects of honeycomb cells by introducing roughness effects on the smooth land. A complete geometrical representation of honeycomb cells was considered in Ref. 4, but the configuration did not include the rotating knife. Ref. 5 proposed an approach of modeling the 3-D honeycomb cells by circumferential grooves. Refs. 6 and 7 addressed a complete configuration consisting of the knives and honeycomb cells, but did not take rotation into account. Ref. 8 considered realistic rotating knife geometries, but excluded the honeycomb cells.

Apart from its potential to reduce risks involved during the development process of a new seal, CFD allows one to gain a thorough insight into the flow processes inside the seal. The continuing development of CFD algorithms, facilitated by the ever increasing performance and cost-effectiveness of computers, opens ample possibilities to incorporate more complete physics into the CFD modeling.

It should be emphasized that the models and conditions tested in the NLR seal test rig facility are highly representative to real-life situations. The facility provides the mass flow value (i.e. the gas leakage) as the primary data for given conditions such as rotational speed, pressure ratio, inlet pressure and inlet temperature. Such data is not suitable for validation of a CFD method on the level of flow field properties such as velocity profiles, pressure distributions, etc., occurring inside the flow.

However, a comparison in terms of the mass flow and pressure ratio between the numerical and experimental data is still useful, provided that the same geometrical details of the seal model in the test rig are also present in the computational domain, while the underlying flow model contains important effects from compressibility, viscosity, turbulence and vortical flow structures.

A close agreement between the numerical and experimental data can then be interpreted as an indication that the flow physics occurring in the test are captured by the CFD method. It should therefore increase confidence about the applicability of the method. *The first objective* of the paper is to perform such a comparison, involving CFD computations for a three-dimensional labyrinth seal with a honeycomb land that closely represents a tested seal model. In contrast to previous works, this paper addresses a case where the honeycomb cells and the rotation are taken into account.

Subsequently, the computational results facilitate a three-dimensional investigation to get a good insight into the flow phenomena in the labyrinth seal. *The second objective* is therefore to present a new approach for exploiting the CFD methodology to investigate the flow characteristics and sealing mechanisms in terms of losses generated in the labyrinth seals. *The third objective* is to demonstrate the suitability of the approach for assessing different seal concepts.

The achievement of complete technological building blocks provides a comprehensive capability not only important to the aircraft engine Original Equipment Manufacturers (OEMs) but also to companies involved in the development and production of seals. The importance lies with achieving better engine and component performance through the reduction of seal leakage at similar or reduced production cost. Accordingly, an industrial perspective towards exploiting the achieved capability is presented.

2 Labyrinth seal test cases

Three test cases are considered. Case-1 concerns a stepped labyrinth seal configuration referred to as the baseline labyrinth seal in the test campaign performed in the NLR seal test rig (Ref. 1). The geometry of the honeycomb cells of this configuration is shown in Figure 1. The labyrinth seal features three straight knives with converging steps. This test case serves the purpose of achieving the first objective mentioned above.

Case-2 concerns a labyrinth seal with a smooth land, which is obtained by taking the honeycomb out of the Case-1 configuration, replacing the mouth of the honeycomb cells by a solid wall. Case-1 and Case-2 serve the purpose of achieving the second objective.

Case-3 considers a labyrinth seal geometry featuring three canted knives with a smooth land. The knives are canted with the same angle towards the incoming flow. No experimental data is available for the smooth land configurations. Case-2 and Case-3 serve the purpose of achieving the third objective. Therefore, Case-3 should not be considered as a variant of Case-2, but as a completely different seal concept resulting from other design considerations.

The knife-edge corners are assumed sharp. The differences between the seal geometries are illustrated in Figure 2, where the geometries are shown on the same scale.

3 CFD method and setup

The Reynolds-Averaged Navier-Stokes equations are employed as the flow governing equations. Turbulence is incorporated by means of the TNT variant of the two-equation k-ω turbulence model (Refs. 10, 11). This variant eliminates the free-stream dependency and the wall singularity of the original Wilcox's k-ω turbulence model. As flows through labyrinth seals are expected to contain vortical structures, a correction scheme is introduced to the turbulence model to avoid excessive dissipation in the vortex core region. This correction scheme in combination with the abovementioned turbulence model has proved to be effective in producing accurate simulation of vortical flows (Ref. 12).

The surface surrounding the domain of the flow through a labyrinth seal can be distinguished into:

- Rotating solid boundary (knives and cylindrical base).
- Static solid boundary (honeycomb cells and shroud).
- Inflow boundary.
- Outflow boundary.
- Side boundaries.

An adiabatic wall and no-slip boundary condition is applied to all solid boundaries. A circumferential velocity is imposed on the rotating solid boundary, while a zero velocity is imposed on the static solid boundary. The momentum calculated from the given mass flow is imposed on the inflow boundary along with the inlet temperature, while the pressure is imposed on the outflow boundary. The swirl at the inflow boundary is set to zero.

The geometrical periodicity of the honeycomb cells implies that only a small part of the labyrinth seal configuration, spanning about 1 degree circumferentially, needs to be taken into account in the computational domain. A circumferential cyclic (periodic) boundary condition is then applied on the side boundaries, ensuring a balance of the conservative fluxes. Figure 3 shows a schematic diagram of the boundaries.

The flow governing equations are discretized by means of a cell-centered finite volume scheme. The physical flow domain is represented by a multi-block computational domain containing structured grids. A pseudo-time integration scheme is applied to the system of equations to provide a steady-state solution inside the domain, accelerated by a multi-grid scheme and local time stepping. Matrix-type artificial dissipation is added to the continuity, momentum and energy equations to ensure stability of the integration scheme as well as accurate capturing of boundary and shear layers.

The solution procedure is provided by NLR's ENSOLV flow solver which is a component of NLR's CFD system ENFLOW (Ref. 9). Other components of ENFLOW are used for the computational setup, namely (i) the domain modeler ENDOMO to develop the multi-block domain topology and assign the boundary conditions, and (ii) the grid generator ENGRID to generate smooth structured grids throughout the flow domain, with the point-to-point connection on the block interface. The grids are appropriately stretched towards the solid wall to sufficiently resolve the boundary layer by the value of y^+ of around unity. Relatively high grid resolution has been made around the knife edge and between the knife and the step wall in order to capture the flow physics. The number of grid cells has been specified to allow 3-level multigrid computations.

For Case-2 and Case-3 the flow domain can be reduced to a two-dimensional (2-D) axisymmetrical computational domain, consisting of about 20,000 grid cells. For Case-1 the

presence of the honeycomb requires a three-dimensional computational domain which strongly increases the number of grid cells compared to the two-dimensional case of Case-2. A grid refinement study results in a number of grid cells of about 10 million.

This grid can sufficiently capture the important flow physics with high gradients around the knife-edge and in the region between the knife and the step. It also covers two buffer zones. One zone is upstream of the first knife to allow the swirl to develop. Another zone is downstream of the third knife to fully capture a large vortex, ensuring the consistency of the boundary condition at the outflow boundary. Figure 4 gives an impression of the grid.

4 Experimental seal-test-rig facility

A high temperature, high speed, high pressure seal test rig with Active Clearance Control (ACC) is available at the National Aerospace Laboratory NLR in the Netherlands (Ref. 1). The layout of the seal test rig including the ACC system with locations of capacitive probes for clearance measurements is shown in Figure 5.

The rig consists of a pressure vessel, made of steel, to hold a pressure up to 24.1 bar (350 psi). The seal test rig is designed to allow internal rig operating gas temperatures up to 816°C (1500°F). The vessel supports a vertically placed shaft with two mounted 254 mm (10 inch) diameter disks. The shaft is driven by an air motor at a maximum speed of 27,500 rpm, resulting in a surface speed of 365 m/s (1200 ft/s) based on the 10-inch diameter. The upper disk, or "hot disk", is the rotating part of the seal to be tested. The hot disk runs inside the non-rotating part (land) of the seal. The lower "cold disk" is used to balance the axial load caused by the pressure difference over the hot disk.

The clearance between the rotating part of the seal and the non-rotating part of the seal is measured at three angular positions using Capacitec(c) proximity probes. Temperature and rotor speed have a strong influence on the size of the clearance between the rotating disk and the non-rotating part of the seal. Therefore an ACC system has been implemented. This system cools the non-rotating part of the seal backing plate structure and reduces its diameter to control the size of the gap.

It should be noted that, because of the cooling involved in the ACC system, the adiabatic wall boundary condition in the CFD setup may not fully represent the actual condition in the test rig. The adiabatic wall has been assumed as no data is available for the heat flux or temperature over the surface.

Also, there is no data on the swirl upstream of the seal. A zero-swirl at the inlet has therefore been assumed. It should be noted that the distance between the inlet and the first knife allows the swirl to pick up a finite value (due to the rotating boundary) while approaching the first knife.

5 Comparison of results

For comparison with the experimental data, CFD computations have been performed for the seal-test-rig conditions and measured data shown in Table 1. The computational procedure can be outlined as follows. The reference pressure and temperature are selected to be equal to the experimental values of the inlet pressure and temperature. The reference density follows from the perfect gas relation. The reference velocity u is obtained from the experimental value of the mass flow W using the relation:

$$W = \rho u A \qquad\qquad (1)$$

where A is the inlet area. These reference quantities are used to determine the reference Mach number and Reynolds number required as input by the flow solver, and to scale the flow variables as the flow solver operates with non-dimensional variables. For each computation, Table 1 provides:

- a Rotation-Per-Minute (RPM) value that determines the non-dimensional circumferential velocity on the rotating boundary,
- a mass flow and inlet temperature to determine the non-dimensional momentum and temperature on the inflow boundary,
- a pressure ratio for the specification of the non-dimensional outlet pressure on the outflow boundary.

The primary output of the computation is the inlet pressure p_i on the inflow boundary. The numerical values of the mass flow function ϕ can then be determined as:

$$\phi = \frac{W\sqrt{T_i}}{p_i A_{gap}} \qquad\qquad (2)$$

and the pressure ratio Π as

$$\Pi = \frac{p_i}{p_o} \qquad\qquad (3)$$

The computational results for the three entries of Table 1 lead to Figure 6, showing a comparison between the experimental data and CFD results. Since the experiment on the test rig and the CFD computation only share the same mass flow, inlet temperature, outlet pressure and rotational velocity (i.e. the quantities appearing in the boundary conditions), the percentage shown in the figure is the maximum of the individual deviations in ϕ and Π. It should be noted that the test rig has an accuracy of ±3.5% for the mass flow function. Also, there are uncertainties in the CFD setup due to the assumptions on the knife-edge corners and the boundary conditions. Within this measurement accuracy and CFD setup uncertainties, the

11

shown deviation of about 1% represents a close agreement between the CFD results and the experimental data.

6 Analysis of Case-1 results

For the first condition in Table 1, an analysis of the flow is given as follows. One way to analyze the sealing properties is through evaluating the total pressure loss that occurs in the flow. Total pressure is defined as:

$$p_t = p \left(1 + \frac{\gamma - 1}{2} M^2 \right)^{\frac{\gamma}{\gamma - 1}} \qquad (4)$$

The total pressure loss is defined in normalized form as:

$$p_{t,loss} = 1 - \frac{p_t}{p_{t,ref}} \qquad (5)$$

where the reference total pressure $p_{t,ref}$ corresponds to the inlet condition.

Figure 7 presents local views of the cavities between two adjacent knives on the mid-plane and side-plane. The geometrical difference between these planes lies in the relative position of the knife edge with respect to the honeycomb cell. On the mid-plane the knife edge is positioned below the cell-mouth, while on the side-plane the knife edge is positioned below the cell wall. For all cavities the span of the contour levels are the same, but the minimum and maximum values are adjusted locally to those occurring within the cavity. There is no significant difference in the pattern of the total pressure loss in the cavities on the different planes.

Each knife edge appears to produce the same amount of losses. Only the orientation, the width and the length of the jet (and therefore the gradient of the losses), and the location with the highest gradient of the losses are different between the planes. These characteristics are determined by the effective gap orientation and width between the knife edge and the cell wall.

Figure 8 shows in-plane streamlines on the mid-plane and side-plane with static pressure contours on the background. It should be noted that these streamlines are not the projection of three-dimensional streamlines. They are constructed using the radial and axial components of the velocity only. There is no significant difference in the pattern of the streamlines, except in the vicinity of the knife-edge reflecting the geometrical differences of the position of the knife edges relative to the honeycomb cells. Near the base, two clearly isolated recirculating regions can be observed in the first cavity and one recirculating region in the second cavity. This can be attributed to the different aspect ratios between the two cavities.

A more elaborate assessment is performed by observing the losses along three-dimensional streamlines. The streamlines are constructed by integration of the velocity vector. Figure 9 shows ten streamlines originating from a rake drawn between the two side boundaries upstream of the first knife-edge. As the flow is steady, the streamline coincides with the particle path (i.e. the streampath). The streamlines are colored with the total pressure loss. This figure shows the different paths taken by the streamlines passing through the cell-mouth and by those passing through the gap.

These paths indicate that the effective distance between the knife-edge and the step may be larger than its geometrical (nominal) step distance. The nominal step distance refers to the distance between the knife-edge and the step in the case of a smooth land (Case-2). The streamline passing through the cell-mouth exhibits a stronger rotational effect. A particle on this streamline travels circumferentially farther to cover the nominal step distance. In contrast, the streamline passing through the gap exhibits a weaker rotational effect and is more axially aligned. Because of the honeycomb structure, a particle on this streamline travels a distance that is about a half-cell width larger than the nominal step distance. One of such streamlines is indicated by an arrow in Figure 9.

Figure 10 shows two streamlines spanning throughout the labyrinth seal configuration. The first streamline with the path ABC, passes the first knife-edge through the gap. When passing the second knife-edge, this streamline enters and leaves the honeycomb cell. The second streamline with the path ADE passes the first knife-edge through the cell-mouth. Clearly the effect of rotation is larger on the second streamline ADE than on the first streamline ABC. The no-slip condition on the honeycomb wall (in the gap) appears to resist the flow from following the rotation of the knife-edge. It should be noted that this pattern of streamlines is repeated in the circumferential direction according to the geometrical periodicity of the honeycomb cell. The streamlines are colored with the total pressure loss (the contour levels are different than those used in Figure 9).

Projecting the three-dimensional streamlines and the geometry of the labyrinth seal on an axial-radial plane results in Figure 11, where curves for the total pressure loss and the turbulence kinetic energy along the streamlines have also been drawn.

When passing the first knife-edge, streamline ABC experiences an abrupt increase of loss at the entrance to the gap where there is an abrupt increase of the turbulence kinetic energy. The loss increases gradually in the shear layer of the jet until it attains the level in the first cavity. Streamline ADE experiences effectively two gaps, the first one being above the first corner of the knife-edge when the streamline goes upward and the second gap is at the second corner after the streamline is bent downward. These locations are characterized by a maximum turbulence kinetic energy where a large increase of the total pressure loss is evident. Both streamlines do not experience any significant loss across the cavity.

When passing through the second knife-edge, a particle on streamline ABC experiences an abrupt increase of the total pressure loss near the upstream corner of the knife-edge. It enters the honeycomb cell afterwards, where only a negligible increase of loss is observed. Finally, another significant increase of loss near the downstream corner of the knife edge is observed when the particle leaves the knife-edge.

Another situation can be observed on the streamline ADE. After spanning over the cavity, the streamline attaches on the surface of the second knife, and follows the surface until it arrives at the knife-edge. The curve indicates a decrease of loss in this area. This decrease can be attributed to the effect of rotation.

The situation at the third knife-edge is opposite to the situation at the first knife-edge, where streamline ABC passes through the cell-mouth and streamline ADE passes through the gap. The phenomena observed around the first knife-edge can also be found here.

7 Analysis of Case-2 results

For this case, the inlet pressure resulting from the 3-D computation of Case-1 for the first condition of Table 1 is used as a target for the same mass flow. In order to match this target, the value of the outlet pressure is determined by an iterative procedure. The target inlet pressure ensures that the inlet total pressure level of Case-2 is equal to that of Case-1, in order to allow a sound comparison of the losses between the two cases.

Figure 12 shows the resulting in-plane streamlines with pressure contours on the background. Compared with Figure 8, there is a significant difference in the flow topology. Without the honeycomb cells, the flow exhibits distinct isolated and stronger circulating regions. Downstream of the third knife-edge, the vortex fills almost the whole channel, while the suction peak in the core is higher with a clockwise rotation.

Figure 13 shows close-up views of the cavities of the total pressure loss, while Figure 14 presents the total pressure loss with the corresponding turbulence kinetic energy along the streamline. The streamline experiences the largest increase of loss at the gap entrance, where the turbulence kinetic energy reaches a maximum. The flow impinges on the knife edge and separates at the upstream corner of the knife-edge. The losses continue to increase while the shear layer impinges on the step wall, is deflected downward following the wall, separates from the wall, attaches on the knife surface and follows the surface of the knife. This additional loss can be attributed to shear-action in the shear layer, and in a lesser extent, to the transfer of momentum that keeps the flow in the recirculating regions rotating and to the viscous effect in the boundary layer on the step wall. Across the cavity there is no significant increase of loss. The results indicate that turbulent mixing and shear give a dominant contribution to the losses.

At the notch (on the upstream side) of the second knife, an additional loss occurs in the shear layer when the flow separates. Afterwards, a similar mechanism occurs as for the streamline passing the first knife edge. At the notch of the third knife, losses can again be observed in the shear layer when the flow separates. The losses that follow can be distinguished into the losses due to turbulent mixing and shear, and afterwards due to the momentum transfer into the large recirculating region downstream of the third knife-edge.

A comparison between Figure 11 and Figure 14 shows that the presence of honeycomb cells significantly reduces the local production of turbulence kinetic energy. Furthermore, the structure of the honeycomb cells prevents the formation of a coherent shear layer around the knife-edge and therefore inhibits a high generation of losses like those occurring in the case of a smooth land. Also, it has made the step much less effective by suppressing the loss-generating flow impingement at and separation from the step wall. Figure 11 suggests that streamlines passing the knife-edge through a cell-mouth may miss the step completely. One should then consider that throughout the circumference of the seal, half of the streamlines passes through a cell-mouth and the other half passes through a gap. It can be observed too that the direction of the rotation and the position of the recirculating region in the cavity prevent the formation of a loss-generating flow separation at the notch on the upstream wall of the knife.

Finally, it can be observed that for the same mass flow, inlet temperature and inlet pressure (and therefore for the same mass flow function ϕ), the labyrinth seal with a smooth land requires a larger pressure ratio of 2.2 compared to about 1.25 when the honeycomb is present, due to the larger loss of the total pressure. This finding is in line with the observation in another study (Ref. 6, 14), where in case of a small ratio between the width or clearance of the knife and the cell size a significant increase of leakage flow is expected.

8 Analysis of Case-3 results

A three-knife-edge labyrinth seal geometry with the knives canted towards the incoming flow is considered. The geometrical differences of the canted-knife labyrinth seal relative to the baseline seal with the straight knives can be identified as follows:

- the shape and volume of the expansion chambers have changed due to the angle of the knives,
- the step heights are larger, such that the annulus area at the outlet is smaller,
- the tip of the canted knife is profiled consisting of two flat surfaces, instead of one flat surface, giving effectively a larger clearance at the upstream corner of the knife,
- the distance between the knife edge and the step wall is larger.

Again, as in Case-2, the inlet pressure resulting from the 3-D computation of Case-1 for the first condition of Table 1 is used as a target for the same mass flow, in order to ensure the same total pressure level at the inlet.

Figure 15 presents the resulting in-plane streamlines with pressure contours on the background, which shows a completely different flow topology from that of Case-2 in Figure 12. The pressure jumps across the knives are smaller. There are now three major recirculating regions in the area between two adjacent knives. Downstream of the third knife-edge, the reattachment occurs earlier, leading to a smaller vortex.

Figure 16 presents separate views of the cavities, while Figure 17 shows the total pressure loss with the corresponding turbulence kinetic energy along the streamline. A similar process as that of the straight knife can be observed. However, turbulence mixing around the knife-edge appears to be less intense. The losses nearby the step are much smaller. The jet flow seems to be too dissipated to cause a significant flow impingement at the step wall. Also, there is only a mild separation at the lower corner of the step wall, leading to only a small increase of the total pressure loss. The losses due to flow separation at the notch seem to be absent too. Interference from the recirculating flow in the cavity seems to be responsible for this absence. Smaller losses behind the third knife can be attributed to smaller extent of turbulence and shear in combination with a smaller vortex. For the same mass flow, inlet temperature and inlet pressure (and therefore for the same mass flow function ϕ), the labyrinth seal with canted knives requires a pressure ratio of 1.8 compared to 2.2 in the case of straight knives.

9 Industrial Perspective

The application of CFD in combination with experimental techniques gives the possibility to obtain more detailed information and in-depth understanding of the complex leakage flow through labyrinth seals. The eventual goal of these studies is to predict the leakage flow through labyrinth seals accurately and cost effectively. During the development of new seal configurations and accompanying (upgrades of) engineering models employing a one-dimensional (1-D) flow solver, the CFD method can be utilized to:

- Determine the sealing benefit of conceptual geometries in order to down select the most promising candidates (possibly supported by rig-testing in limited design space).
- Identify relevant leakage parameters for proposed geometries.
- Determine the sealing benefit of detailed geometries with validation in advanced test-rig under engine-like conditions.
- Support the correct representation of test-data into semi-empirical engineering models (e.g. by providing detailed information of loss mechanisms).
- Extrapolate correlations for the engineering models to a limited extent beyond the measured range of test-data.

With the increasing performance of computers, a simplified 2-D CFD model could predict seal flows in less than an hour on a standard PC, while a detailed 3-D CFD model could provide simulation data in an overnight job on a mainframe computer. For the design of labyrinth seals this is too elaborate and engineering models are still preferred to maximize cost effectiveness of the analysis. One way to incorporate CFD in seal design is to use the simulation results and create a database for an engineering model (in a fashion like presented in Ref. 13). Compatibility with internal flow network solvers and the need for validated tools to reduce risk will generally limit the involvement of stand-alone CFD in seal design to specific cases. The role and added value of CFD is therefore most pronounced during the technology development phase.

10 Conclusions

Referring to the three objectives set out in the introduction, based on the obtained results for the seal configurations and flow conditions investigated, the following conclusions can be drawn. First, the comparison between the results of the CFD computation and the experimental measurement shows a close agreement. This is an indication that the important flow physics responsible for the sealing mechanism have been captured by the CFD method.

Second, an analysis of the flow topology and the losses experienced along the streamlines has been performed. This approach reveals that the sealing mechanism of the flow through labyrinth seals is due to losses associated with turbulent mixing and shear which dominantly occur in the vicinity of the knife edge and to a lesser extent around the step wall. For the straight three knife-edge configuration considered, the effects of the honeycomb can be identified as decreased production of losses due to:

- less intense turbulent mixing around the knife-edge,
- preventing the formation of a coherent shear layer,
- mitigating the flow impingement on the step wall,
- inhibiting flow separations at the notch.

Third, from comparing two different seal concepts, the lower performance of the canted-knife seal concept with respect to the straight-knife concept can be attributed to mitigated flow impingement on the step wall, absence of flow separations from the notch, and less intense turbulent mixing and shear in the vicinity of the knife-edge.

Finally, industrial perspectives have been presented to outline the importance of the CFD method, complementary to the seal test rig facility, in particular during the development of seal technology.

Acknowledgments

References

1. G.A. Kool et al, Advanced seal test rig validation and operation, Paper GT2006-90915, 2006.
2. D. Rhode, S. Ko, S., and G. Morrison, Leakage optimization of labyrinth seals using a Navier-Stokes code, Tribology Transaction 37, 1994.
3. D.C.J. Allcock, P.C. Ivey, and J.R. Turner, Abradable stator gas turbine labyrinth seals Part 1: Experimental determination and CFD modelling of effective friction factors for honeycomb materials. AIAA-2002-3936 Paper, 2002.
4. G. Chochua, W. Shyy, and J. Moore, Computational modeling for honeycomb-stator gas annular seal, Intl. J. Heat and Mass Transfer 45, 2002.
5. D-C, Choi and D.L. Rhode, Development of a 2-D CFD approach for computing 3-D honeycomb labyrinth leakage, GT2003-38238 paper, 2003.
6. V. Schramm, K. Willenborg, S. Kim, and S. Wittig, Influence of a Honeycomb Facing on the Flow Through a Stepped Labyrinth Seal, Trans. ASME - A - Engineering for Gas Turbines and Power, vol. 124, pp 140-146, January 2002.
7. D. Collins et al, Numerical modelling of three dimensional honeycomb labyrinth seals employing a simplified approach, GT2006-90850 Paper, 2006.
8. R. Paolillo et al, Rotating seal rig experiments: test results and analysis modelling, GT2006-90957 Paper, 2006.
9. J.W. Boerstoel, A. Kassies, J.C. Kok, and S.P. Spekreijse. ENFLOW, A full-functionality system of CFD codes for industrial Euler/Navier-Stokes Flow Computations. NLR TP 96286 (presented at the 2nd Int. Symp. on Aeron. Science and Tech., Jakarta, 1996).
10. J.C. Kok. Resolving the dependence on freestream values for the k-ω turbulence model. AIAA Journal, 38(7), pp. 1292–1294, 2000.
11. J.C. Kok and S.P. Spekreijse. Efficient and accurate implementation of the k-ω turbulence model in the NLR multi-block Navier-Stokes system. NLR TP-2000-144 (presented at ECCOMAS 2000, Barcelona, Spain, 11-14 September, 2000).
12. F.J. Brandsma, J.C. Kok, H.S. Dol, A. Elsenaar, Leading edge vortex flow computations and comparison with DNW-HST wind tunnel data. NLR TP-2001-238 (RTO/AVT Vortex Flow Symposium, Loen, Norway, 2001).
13. D.C.J. Allcock, P.C. Ivey, and J.R. Turner, Abradable stator gas turbine labyrinth seals Part 2: Numerical modelling of different seal geometries and the construction of a second generation design tool, AIAA-2002-3937, 2002.
14. Stocker, H.L., Cox, D.M. and Holle, G.F.; "Aerodynamic Performance of Conventional and Advanced Design Labyrinth Seals with Solid-Smooth, Abradable and Honeycomb Lands", NASA CR-135307, 1977.

Inlet temperature (C)	Inlet pressure (kPa)	pressure ratio	mass flow (kg/s)	speed (rpm)	clearance (mm)
600	1200	1.25	0.165	12956	0.252
599	1199	1.40	0.184	12937	0.263
600	1200	1.60	0.223	12983	0.266

Table 1 Computed seal-test-rig conditions.
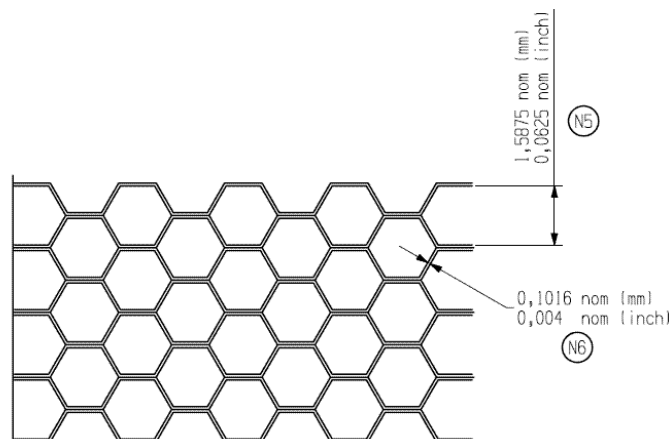
Figure 1 Honeycomb geometry (Case-1).

Case-1

Case-2 (identical with Case-1 without honeycomb)

Case-3
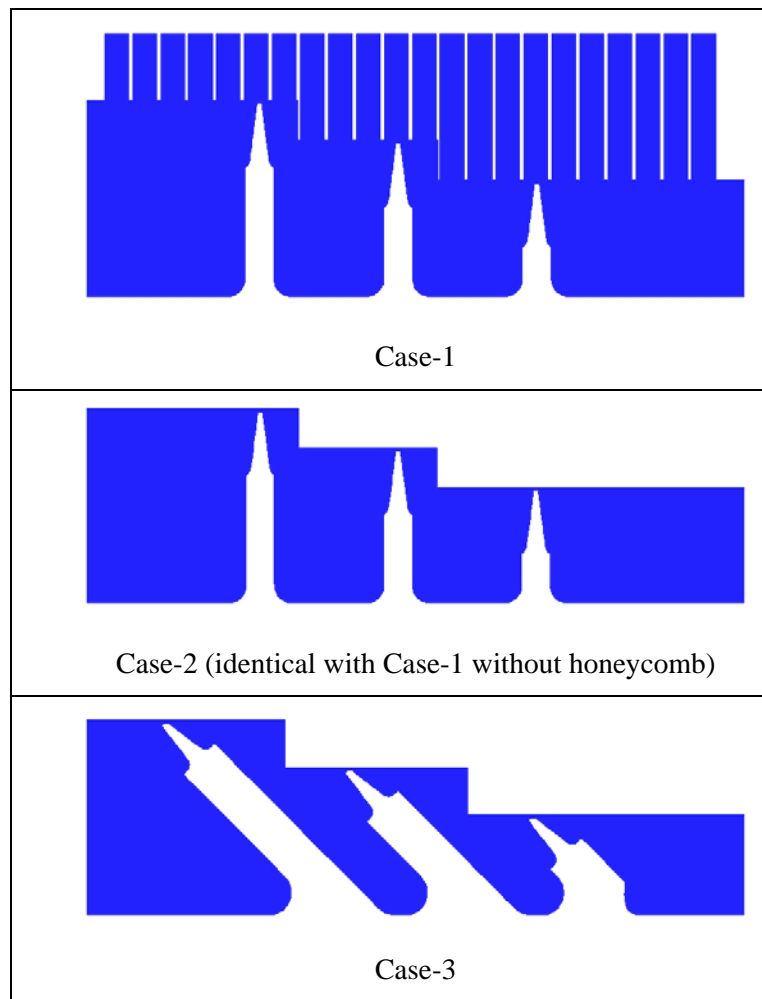
Figure 2 Labyrinth seal configurations (all geometries are shown on the same scale; the direction of the flow is from left to right).
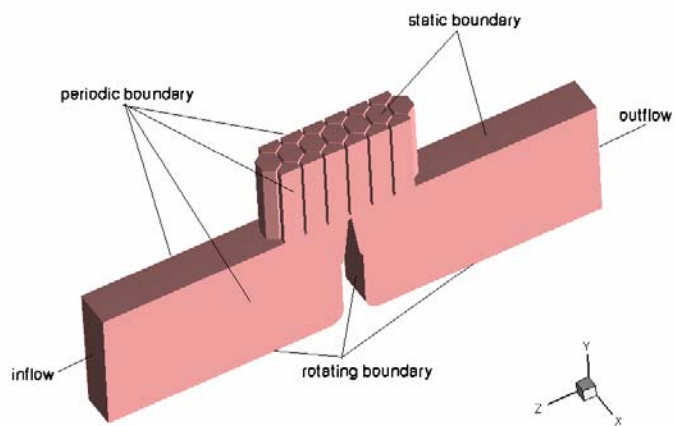
Figure 3 Schematic diagram of the boundaries.

20
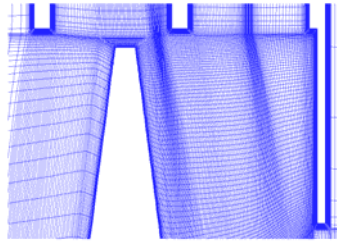
(a) close-up view around the knife-edge
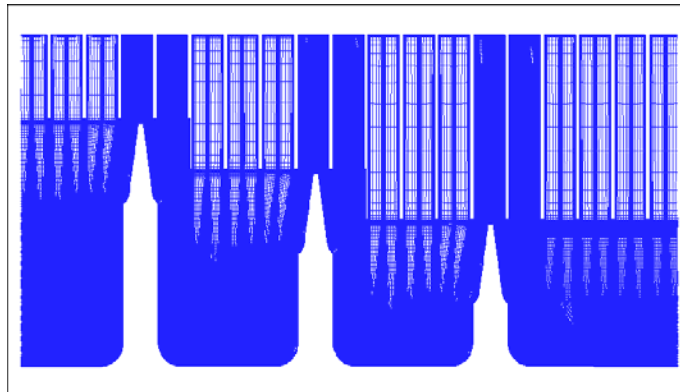
(b) mid-plane view

**Figure 4 Impression of the computational grids
(Case-1).**
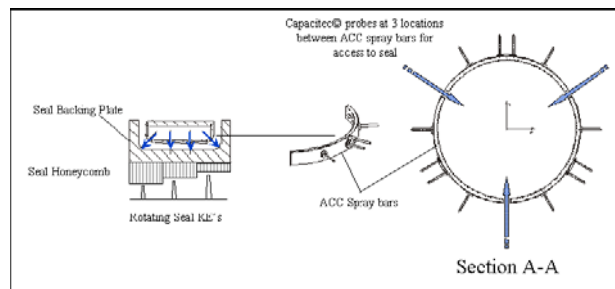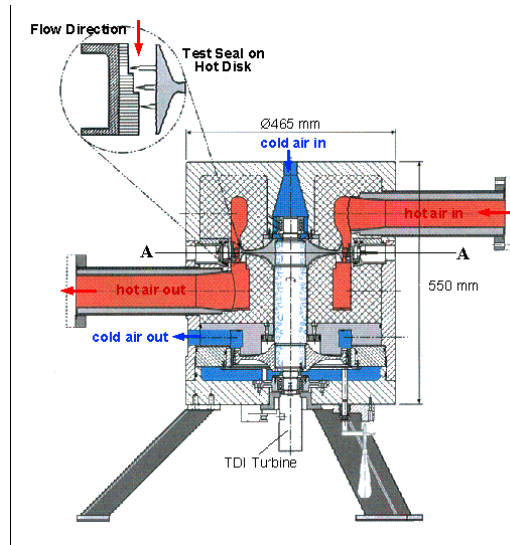
Figure 5 Cross-section of NLR's advanced seal test rig.
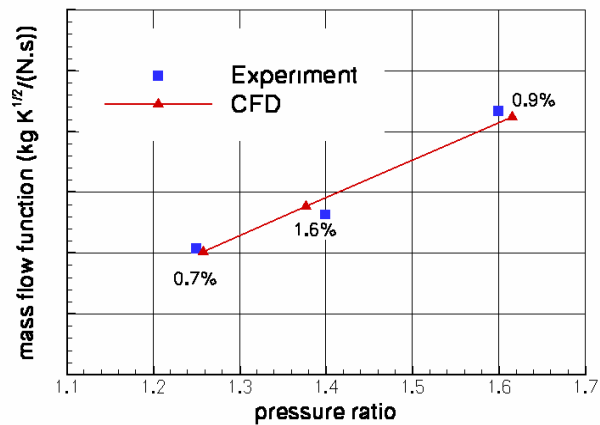
Figure 6 Comparison of engineering model, experimental and CFD results (Case-1).
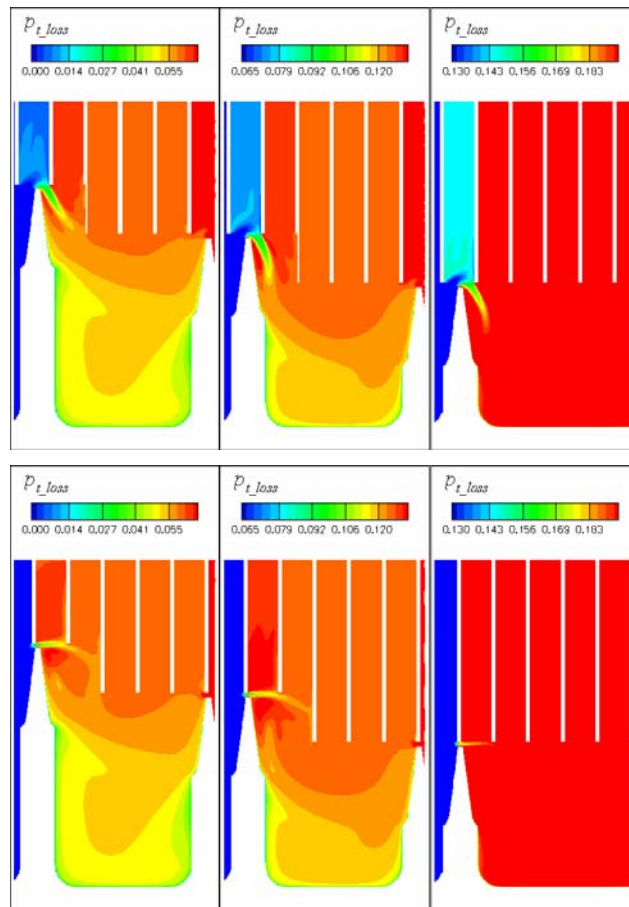
Figure 7 Total pressure loss contours in the cavities on the mid-plane (upper) and side-plane (lower) (Case-1).
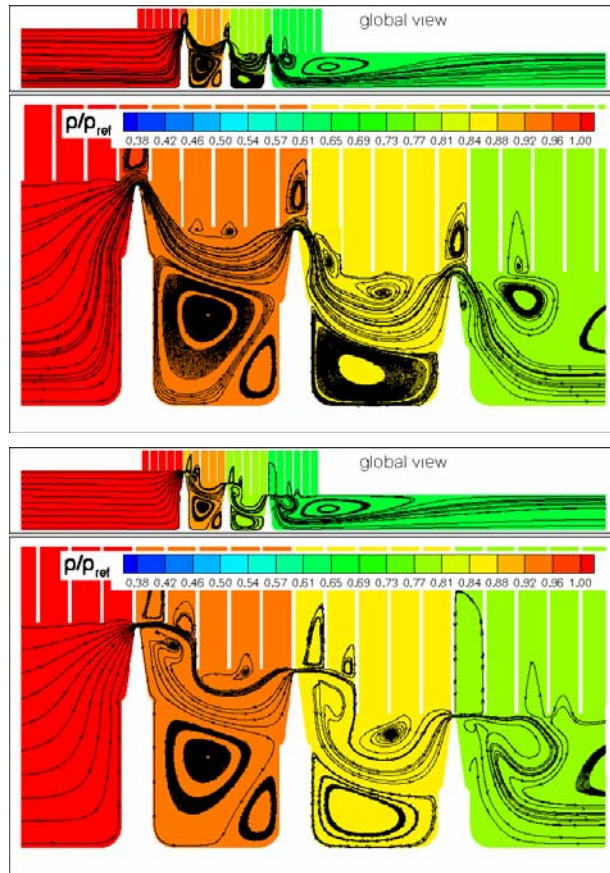
Figure 8 In-plane (two-dimensional) streamlines on the mid-plane (upper) and side-plane (lower) with pressure contours (Case-1).
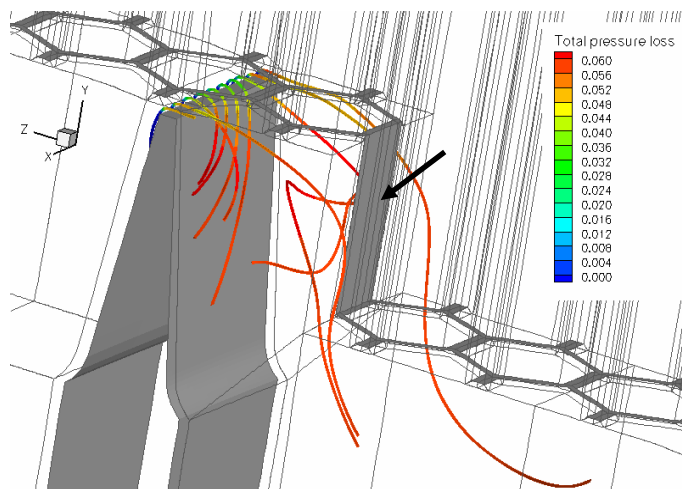
Figure 9 Variation of the total pressure loss along the streamlines across the first knife-edge (Case-1).
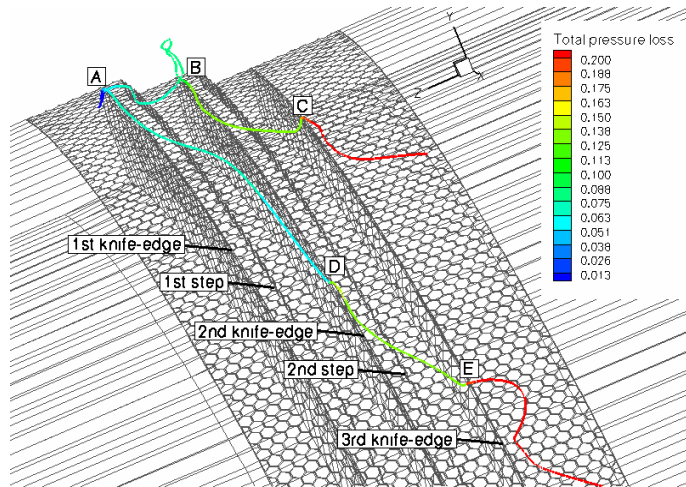
Figure 10 Two streamlines with different paths across the knife-edge (Case-1).
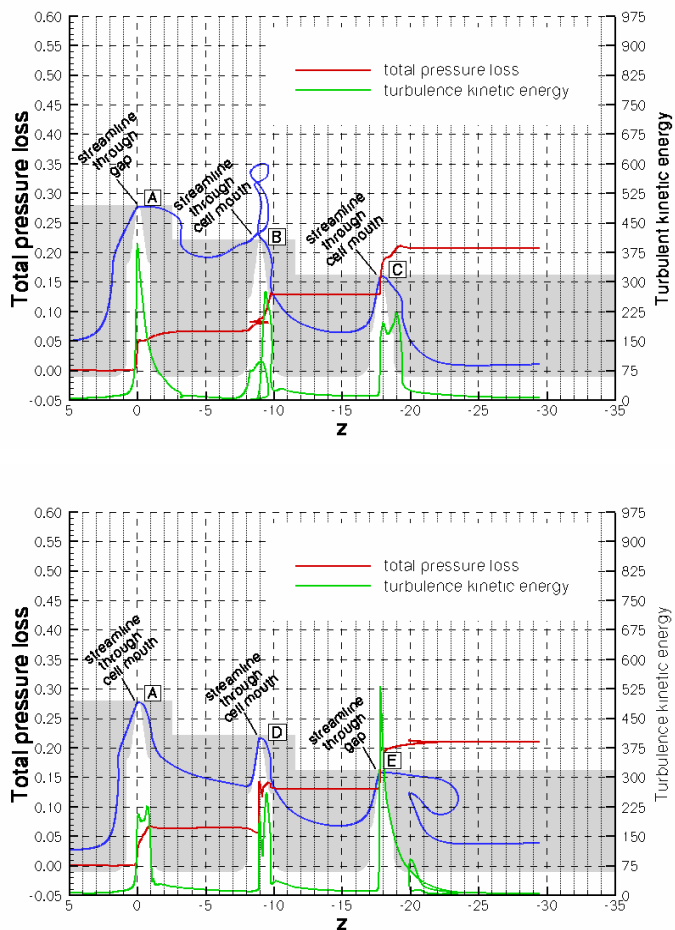
Figure 11 Variation of the total pressure loss (red) and turbulence kinetic energy (green) along the streamlines (blue) following the path ABC and ADE shown in Figure 10 (Case-1).

25
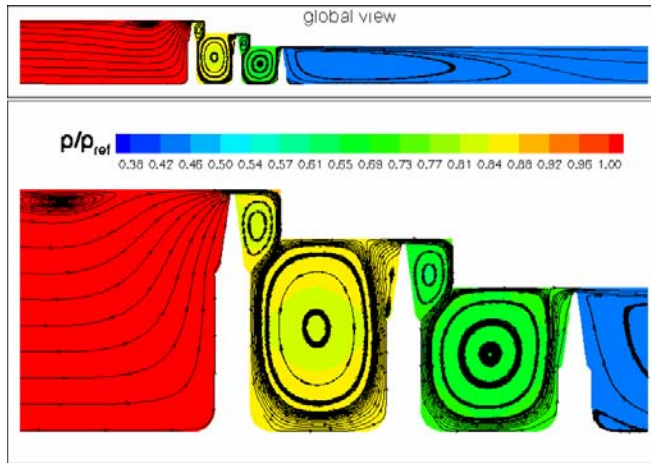
Figure 12 In-plane streamlines with pressure contours (Case-2).
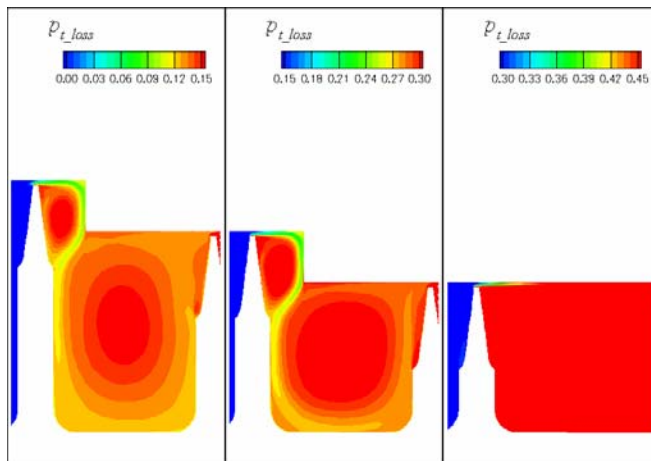
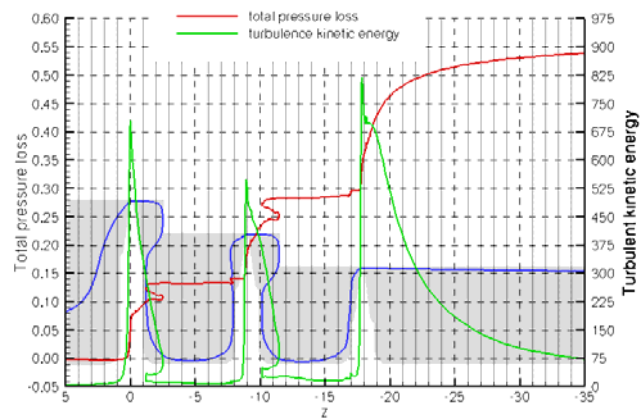**Figure 13 Close-up views of the cavities with contours of the total pressure loss (Case-2).**

Figure 14 Variation of the total pressure loss (red) and turbulence kinetic energy (green) along the streamline (blue) (Case-2).
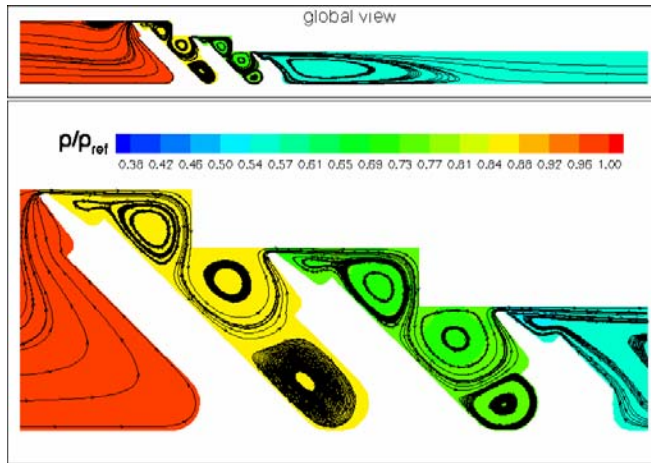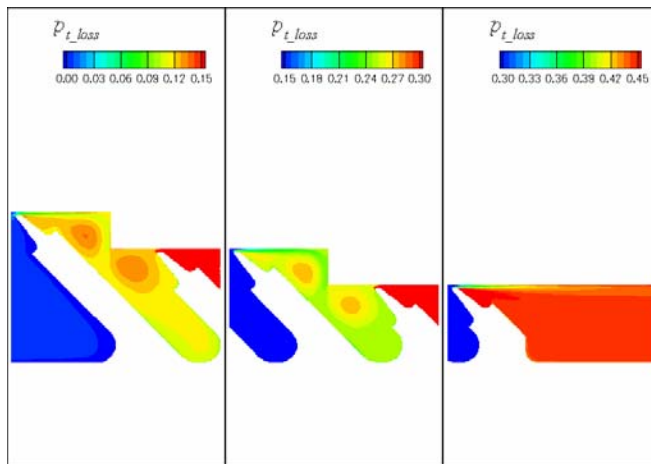
26

Figure 15 In-plane streamlines with pressure contours (Case-3).

Figure 16 Close-up views of the cavities with contours of the total pressure loss (Case-3).
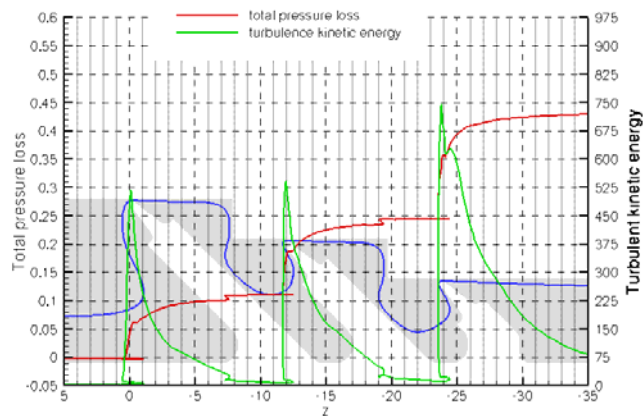

Figure 17 Variation of the total pressure loss (red) and turbulence kinetic energy (green) along the streamline (blue) (Case-3).

27